Hindawi Publishing Corporation
BioMed Research International
Volume 2014, Article ID 586060, 5 pages
http://dx.doi.org/10.1155/2014/586060

Hindawi

Research Article

Effect of Intraocular Lens Diameter Implanted in Enucleated Porcine Eye on Intraocular Pressure Induced by Scleral Depression

Gaku Terauchi,[1] Celso Soiti Matsumoto,[1,2] Kei Shinoda,[1] Harue Matsumoto,[2] and Atsushi Mizota[1]

[1] *Department of Ophthalmology, Teikyo University School of Medicine, 2-11-1 Kaga, Itabashi-ku, Tokyo 173-8605, Japan*
[2] *Matsumoto Eye Clinic, 50-2 Takagaki, Awa-cho, Awa-shi, Tokushima 771-1705, Japan*

Correspondence should be addressed to Kei Shinoda; shinodak@med.teikyo-u.ac.jp

Received 28 December 2013; Accepted 2 March 2014; Published 27 March 2014

Academic Editor: Toshihide Kurihara

The effect of the diameter of an intraocular lens (IOL) implanted in enucleated porcine eyes on the intraocular pressure induced by scleral depression was investigated. Two IOLs of 6 mm and 7 mm optic diameter were implanted. The intraocular pressure (IOP) was monitored during scleral depression by a transducer placed in the midvitreous through a sclerotomy at 6 o'clock. The area under the curve (AUC) of the IOP changes from the beginning of the indentation to the point when the peripheral retinal surface was observed through the IOL optics was measured. The AUC was significantly larger in eyes with a 6 mm IOL than in eyes with a 7 mm IOL ($p < 0.05$). The IOP elevation at the endpoint was higher in eyes with the 6 mm IOL than in eyes with the 7 mm IOL. We conclude that the AUC may represent the degree of stress induced by scleral depression. The higher AUC value with the X-60 may be because of the longer distance from the peripheral retina to the edge of the IOL optics.

1. Introduction

Small-incision cataract surgery and microincision transconjunctival vitrectomy have allowed combining pars plana vitrectomy with phacoemulsification and intraocular lens (IOL) implantation with less time and less invasion [1, 2]. In cases where the IOL is implanted first, the fundus visibility is improved by the clear IOL. However, the edge of the optics of the IOL can interfere with the observation of the equatorial and more peripheral areas of the retina. To overcome this limited view, scleral depression is used to observe the peripheral fundus [3, 4]. Scleral depression is a useful procedure; however, considerable pressure may be required to bring the peripheral retina and vitreous base into view. Scleral depression can be traumatic, because the eye is distorted and the intraocular pressure (IOP) is transiently elevated. However, the effect of scleral depression on the IOP has not been evaluated quantitatively.

Thus, the purpose of this study was to evaluate quantitatively the effects of the IOL diameter on the IOP induced by scleral depression to observe the peripheral fundus. To accomplish this, we implanted a pressure transducer in the vitreous and, also, implanted IOLs into enucleated porcine eyes. The IOP was then measured during scleral depression.

2. Materials and Methods

Combined pars plana vitrectomy, lens aspiration, and IOL implantation were performed on 4 enucleated porcine eyes (Figure 1). We implanted either the eternity X-60 or the eternity X-70 IOLs (Santen Pharmaceuticals, Osaka, Japan) into the porcine eyes. The diameter of the optics was 6.0 mm in the X-60 and 7.0 mm in the X-70 IOL. After the core vitreous was removed, a pressure transducer (Portable, 2-Channel, Serial Port I/O Module, Motorola Solutions Japan Ltd, Tokyo, Japan) was placed into the midvitreous through a sclerotomy at 6 o'clock. Scleral depression was performed at 10 mm posterior from corneal limbus at 3 or 9 o'clock. Constant pressure was delivered to the inner cylinder of a disposable 1cc syringe.

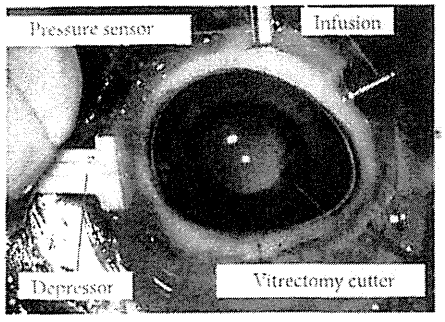

FIGURE 1: Photograph of enucleated porcine eye showing the experimental setup. After combined pars plana vitrectomy, lens aspiration, and IOL implantation, a pressure sensor was introduced into the vitreous cavity through a sclerotomy at 6 o'clock. Scleral depression was performed at 10 mm posterior from the corneal limbus at 3 or 9 o'clock.

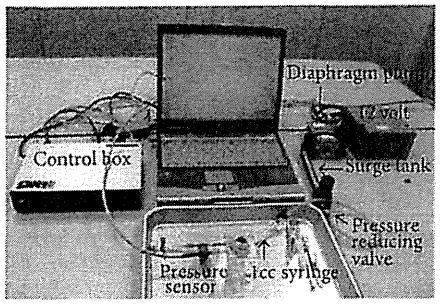

FIGURE 2: A custom made system to deliver constant pressure. Constant pressure (40 mm Hg) was delivered to the inner cylinder of a disposable 1cc syringe, which was used as a scleral depressor. And the external cylinder was held so that the tip of the inner cylinder was just touching the sclera 10 mm posterior from corneal limbus by surgeons.

And the external cylinder was held by surgeons (Figure 2). Physiological salt solution was used for the infusion solution, and the bottle height of the infusion was kept at 40 cm above the eye. To minimize the influence of the pupil diameter on the peripheral retinal observation through the optics, enucleated porcine eyes with similar pupil diameter was used. The apparent pupil diameter (mm) through cornea was 10.92 and 11.01 in eyes with X-60 and 10.96 and 10.98 in eyes with X-70.

The intraocular pressure (IOP) was monitored during scleral depression, in eyes with X-60, 9 times and, in eyes with X-70, 8 times. The IOP was measured from the beginning of the indentation to the endpoint when the peripheral retina was visible through the IOL optics. Then the IOP values were plotted as a function of time, and the area under the curve was determined.

2.1. Statistical Analyses. The AUC during scleral depression and the time from the beginning to the endpoint when the peripheral retina were visible through the IOL optics, and the IOP elevation at the endpoint was measured, unpaired t tests were used to determine the significance of the differences of these parameters between eyes with the eternity X-60 and the eternity X-70. A $p < 0.05$ was taken to be significant.

TABLE 1: Comparisons of the scleral depression parameters between eye with X-60 and X-70.

IOL size	AUC	Δt	ΔP
X-60	908.5 ± 244.1	9.8 ± 2.08	50.5 ± 4.51
X-70	303.5 ± 40.2	7.26 ± 1.11	37.0 ± 1.92
p	$p < 0.01$	$p = 0.29$	$p < 0.01$

Each value is shown as mean ± S.E.
IOL: intraocular lens, AUC: area under the curve.

3. Results

Representative graphs of the IOP change during sclera depression of the eye are shown in Figures 3 and 4. The mean ± standard error of the means (SEM) AUC was 908.5 ± 244.1 mm Hg sec in eyes with the eternity X-60 and 303.5 ± 40.2 mm Hg sec in eyes with the eternity X-70 ($p < 0.01$, Table 1). The time from the beginning to the endpoint when the peripheral retina was visible was 9.8 ± 2.1 sec in eyes with the X-60 and 7.3 ± 1.1 sec in eyes with the X-70 IOL ($p = 0.29$, Table 1) during the sclera depression when great care was taken to exert uniform pressure. The IOP elevation at the endpoint was 50.5 ± 4.5 mm Hg in eyes with the X-60 and 37.0 ± 1.9 mm Hg in eyes with the X-70 ($p < 0.01$, Table 1).

4. Discussion

Scleral depression is used to examine the peripheral retina and also during the shaving of the peripheral vitreous, endolaser photocoagulation of the peripheral retina, and dissection or removing of peripheral membranes. Although endoscopy can be used to avoid scleral indentation, it requires experience and skill. Another solution to the stress on the eye by scleral depression may be to perform the IOL implantation after the vitrectomy or selecting a large diameter IOL [5, 6]. Several authors have reported that an IOL with relative large diameter was advantageous, because the peripheral fundus was visible during the vitreous surgery [5, 6]. With smaller diameter IOLs, the fundus is viewed sometimes through the optics and other times around the optics. Thus, there is a need for continuous refocusing of the operating microscope.

The effect of the IOL diameter on the changes in the IOP induced by scleral depression had not been evaluated. Our results showed that the AUC was smaller and the time to reach the endpoint was shorter with the larger diameter IOL during scleral depression. This is probably because the distance between the peripheral retinal surface and the edge of the IOL optics is farther in eyes with the smaller diameter IOL, and, therefore, a deeper indentation is necessary to bring the peripheral retina into view through the IOL optics. Our results suggest that larger diameter IOL may be able to reduce the depth of scleral indentation, thereby, minimizing the stress on the eye during scleral depression.

Our findings suggest that the AUC may be used to determine the degree of stress on the eye during scleral depression.

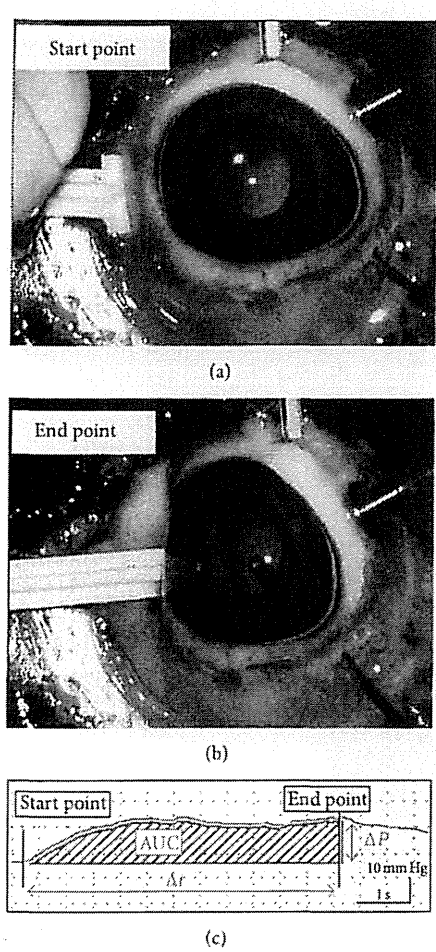

FIGURE 3: Representative graph showing IOP changes during scleral indentation in eye with X-60 implanted. (a) Scleral depression was performed at 10 mm posterior from the limbus at 3 or 9 o'clock. (b) Scleral depression was performed so that the peripheral retina can be seen through the optics of X-60 implanted in the anterior chamber. The markings of the graph show that the starting (arrowhead) and end (arrow) points of the scleral depression are shown in the lower figure. (c) Graph of the intraocular pressure (IOP) as a function of time during the scleral indentation. The area under the curve (AUC) of the IOP from the beginning of the indentation (start point) to the endpoint when the peripheral retinal surface was observed through the IOL was measured. Abscissa axis: time (0.5 seconds/scale), vertical axis: intraocular pressure (10 mm Hg/scale).

The system may also be used for surgeon's exercise for scleral depression.

There are some limitations in our study. Scleral depression was performed with great care to exert uniform pressure. But the speed and pressure depended on the surgeon's experience. The results showed that ΔP was significantly different between eyes with the X-60 and eyes with the X-70 IOL but Δt was not significantly different. This might suggest that the speed rather than the pressure was constant during depression. Constant pressure during scleral indentation by using a syringe pump like system would enable more precise comparison of the IOP change between each indentation. Due to the study design, the surgeon could not be masked to the type of IOL implanted. In addition, the IOP elevation during scleral indentation is influenced by several factors, such as the size of the eye, the rigidity of the eye wall, the position of the indentation, and the material filling the vitreous cavity. We believe that similar results can be observed in the clinical setting, because the size and rigidity of the eye of the porcine eye are not so different from the human eye. In our experiment, the scleral depression was done at 10 mm posterior from the limbus and the IOP change during indentation was measured after core vitrectomy. These procedures are similar to the clinical situation and care was taken to keep these factors constant. It would be interesting to measure the IOP change during scleral indentation when the vitreous cavity is filled with other materials such as air, silicone oil, and perfluorocarbon liquid or during fluid/air exchange.

Recently introduced vitrectomy system (Alcon Constellation Vision System) is equipped with a pressure control system and can maintain IOP at constant, independent of aspiration flow rates during vitrectomy. The IOP control system takes several seconds during the process of IOP detection and feedback [7]. Our system measures the IOP directly

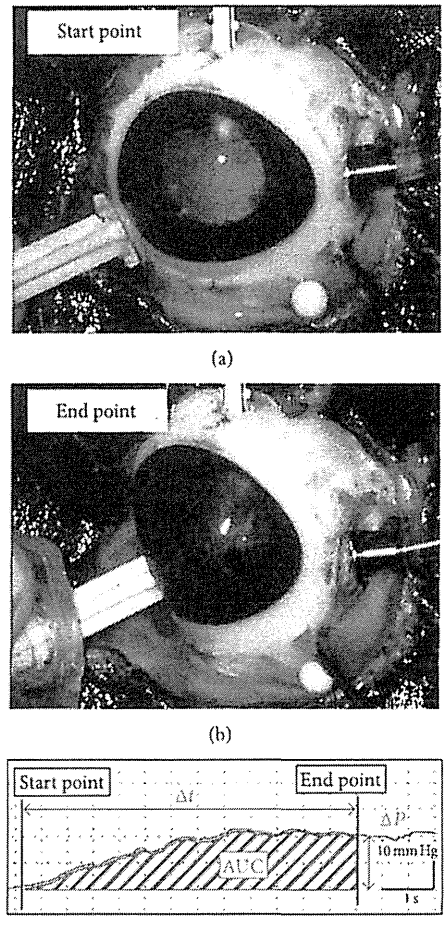

FIGURE 4: Representative plot of the IOP changes during scleral indentation in eye with X-70 IOL implanted. (a) Scleral depression was performed at 10 mm posterior from corneal limbus at 3 or 9 o'clock. (b) The scleral indentation was performed so that the peripheral retina can be seen through the optics of a X-70 IOL implanted in the anterior chamber. The markings of the plotting show that the starting (arrowhead) and end (arrow) points of the scleral indentation are shown in the lower figure. (c) Graph of the IOP as a function of time. The area under the curve (AUC) of the IOP from the beginning of the indentation to the endpoint when the peripheral retinal surface was observed through the IOL optics was measured. Abscissa axis: time (0.5 seconds/scale), vertical axis: intraocular pressure (10 mm Hg/scale).

and does not have such an inherent time lag. Sugiura et al. reported that IOP rapidly increased to 70–100 mm Hg and then slowly decreased to 30 mm Hg in 3.5–4.0 seconds during scleral depression without aspiration, with or without the IOP control system. If the IOP change against the time can be plotted, the AUC may be used as a parameter reflecting the degree of stress of the eye during vitrectomy maneuvers.

In conclusion, we were able to measure the IOP during scleral depression in enucleated porcine eyes implanted with different diameter IOLs. Analysis of the IOP changes clearly showed that an IOL with larger optics can minimize the effects of the scleral indentation.

Conflict of Interests

The authors declare that there is no conflict of interests regarding the publication of this paper.

Acknowledgments

No author has financial or proprietary interest in any materials or methods mentioned. Support of this study was provided by Research Grants on Sensory and Communicative Disorders from the Ministry of Health, Labor, and Welfare, Japan.

References

[1] V. Sood, R. Rahman, and A. K. Denniston, "Phacoemulsification and foldable intraocular lens implantation combined with 23-gauge transconjunctival sutureless vitrectomy," *Journal of Cataract and Refractive Surgery*, vol. 35, no. 8, pp. 1380–1384, 2009.

[2] H. Shinoda, K. Shinoda, S. Satofuka et al., "Visual recovery after vitrectomy for macular hole using 25-gauge instruments," *Acta Ophthalmologica*, vol. 86, no. 2, pp. 151–155, 2008.

[3] I. J. Constable and M. Nagpal, "Proliferative vitreoretinopathy," in *Retina*, S. Ryan, Ed., vol. 3, pp. 1807–1825, Elsevier, New York, NY, USA, 5th edition, 2008.

[4] T. G. Murray, H. C. Boldt, H. Lewis, G. W. Abrams, W. F. Mieler, and D. P. Han, "A technique for facilitated visualization and dissection of the vitreous base, pars plana, and pars plicata," *Archives of Ophthalmology*, vol. 109, no. 10, pp. 1458–1459, 1991.

[5] A. Watanabe, K. Okano, T. Shibata, H. Kato, and H. Tsuneoka, "Clinical efficacy of 7 mm intraocular lens for combined pars plana vitrectomy, phacoemulsifi cation and intraocular lens implantation," *J-Eye*, vol. 26, pp. 1413–1415, 2009 (Japanese).

[6] M. Wakabayashi, A. Imai, N. Kitazawa, D. Chiba, J. Arai, and T. Murata, "The Merits of 7.0 mm optics intraocular lens in phacovitrectomy," *Japanese Journal of Ophthalmology*, vol. 23, no. 1, pp. 121–124, 2010 (Japanese).

[7] Y. Sugiura, F. Okamoto, Y. Okamoto, T. Hiraoka, and T. Oshika, "Intraocular pressure fluctuation during microincision vitrectomy with constellation vision system," *American Journal of Ophthalmology*, vol. 156, no. 5, pp. 941–947, 2013.

Molecular Vision 2013; 19:1580-1590 <http://www.molvis.org/molvis/v19/1580>
Received 1 April 2013 | Accepted 15 July 2013 | Published 20 July 2013

Molecular characteristics of four Japanese cases with *KCNV2* retinopathy: Report of novel disease-causing variants

Kaoru Fujinami,[1,2] Kazushige Tsunoda,[1] Natsuko Nakamura,[1] Yu Kato,[1] Toru Noda,[1] Kei Shinoda,[3] Kaoru Tomita,[4] Tetsuhisa Hatase,[5] Tomoaki Usui,[6] Masakazu Akahori,[1] Takeshi Itabashi,[1] Takeshi Iwata,[1] Yoko Ozawa,[2] Kazuo Tsubota,[2] Yozo Miyake[1,7]

[1]National Institute of Sensory Organs, National Tokyo Medical Center, Tokyo, Japan; [2]Department of Ophthalmology, Keio University, School of Medicine, Tokyo, Japan; [3]School of Medicine, Teikyo University, Tokyo, Japan; [4]Heiwa Ganka Clinic, Tokyo, Japan; [5]Graduate School of Medical and Dental Sciences, Niigata University, Niigata, Japan; [6]Akiba Eye Clinic, Niigata, Japan; [7]Aichi Medical University, Aichi, Japan

Purpose: To describe the molecular characteristics of four Japanese patients with cone dystrophy with supernormal rod responses (CDSRR).

Methods: Four individuals with a clinical and electrophysiological diagnosis of CDSRR were ascertained. The pathognomonic findings of the full-field electroretinograms (ERGs) included a decrease in the rod responses, a square-shaped a-wave, an excessive increase in the b-wave in the bright flash responses, and decreased cone-derived responses. Mutational screening of the coding regions and flanking intronic sequences of the potassium channel, subfamily V, member 2 (*KCNV2*) gene was performed with bidirectional sequencing. The segregation of each allele was confirmed by screening other family members. Subsequent in silico analyses of the mutational consequences for protein function were performed.

Results: There were two siblings from one family and one case in each of the two families. One family had a consanguineous marriage. Mutational screening revealed compound heterozygosity for the two alleles, p.C177R and p.G461R, in three patients, and homozygosity for complex alleles, p.R27H and p.R206P, in one patient from the consanguineous family. There were three putative novel variants, p.R27H, p.C177R, and p.R206P. The four variants in the families with *KCNV2* were highly conserved in other species. In silico analyses predicted that all of the missense variants would alter protein function.

Conclusions: Biallelic disease-causing variants were identified in four Japanese patients with CDSRR suggesting that the pathognomonic electrophysiological features are helpful in making a molecular diagnosis of *KCNV2*. Three novel variants were identified, and we conclude that there may be a distinct spectrum of *KCNV2* alleles in the Japanese population.

Patients with cone dystrophy and supernormal rod electroretinograms (ERGs) were first reported in 1983, and the abnormality in the ERGs indicated a progressive degeneration of the cone photoreceptors associated with unique rod system abnormalities [1]. More detailed characteristics of this rare, autosomal recessive condition were reported in later studies, and the disease was named cone dystrophy with supernormal rod responses (CDSRR; MIM #610356) [2-8].

Most cases with CDSRR typically present in the first two decades of life with reduced visual acuity, abnormal color vision, and photophobia [8-11]. Night blindness is a later feature of the disorder [8]. The fundus appearance is variable, with some having a normal peripheral retina and a range of macular abnormalities [8-10]. The pattern of the autofluorescence (AF) images is also variable: Young cases have either a normal pattern or small parafoveal ring enhancements, while older cases have a narrow high-signal annulus that can encircle a central atrophic area of the retinal pigment epithelium (RPE) [6,12]. Recently, spectral domain optical coherence tomography (SD-OCT) and adaptive optics scanning laser ophthalmoscope (AOSLO) studies have described morphological changes of the fovea even at the early stages [10,13,14].

The electrophysiological findings are pathognomonic of CDSRR, and they assist in its early diagnosis [3,5,8-12,15-17]. The light-adapted ERGs are usually delayed and decreased in keeping with a generalized cone system dysfunction. There is also a unique rod system abnormality; the dark-adapted ERGs elicited by dim flashes are markedly decreased and delayed, and increasing the flash intensity results in an excessive increase in the b-wave amplitude accompanied by a shortening of the peak time of the b-wave [8,9,11]. A square-shaped a-wave trough of the dark-adapted bright flash ERGs is also a characteristic feature of this disorder [9,11].

Correspondence to: Kazushige Tsunoda, Laboratory of Visual Physiology, National Institute of Sensory Organs, 2-5-1 Higashigaoka, Meguro-ku, Tokyo 152-8902, Japan; Phone: +81334110111; FAX: +81334110185; email: tsunodakazushige@kankakuki.go.jp

CDSRR has been shown to be caused by mutations in the potassium channel, subfamily V, member 2 (*KCNV2*) gene (MIM# 607,604), which encodes a voltage-gated potassium channel subunit, Kv8.2 [18]. This silent subunit is expressed in rod and cone photoreceptors [18-20], and is thought to assemble with other K^+ channel subunits such as KCNB1, KCNC1, and KCNF1. These subunits form functional heteromeric channels with altered properties that have a narrowed membrane potential for activation and slow inactivation kinetics [19]. Eventually, these kinetic properties result in transient hyperpolarization overshoots on rapid changes in the inward currents [19]. A deficiency of Kv8.2 by a mutation in *KCNV2* may affect the characteristics of the I_{kx} as first described in amphibian photoreceptors [21]. This deficiency may influence the photoreceptor membrane potential. However, the underlying mechanisms that fully explain the clinical features of CDSRR are still not determined.

More than 50 different disease-causing variants in *KCNV2* have been reported: small insertion and deletion changes or large deletions that constitute a protein truncation and single nucleotide changes with amino acid substitutions [9,10,13,14,16,18,22,23]. Three small case series describe the clinical features of CDSRR in East Asians [3,5,15]; however, molecular genetic studies of these populations have not been published. Thus, the purpose of this study was to determine the molecular genetic characteristics from the clinical and electrophysiological findings of four Japanese patients who were diagnosed with CDSRR.

METHODS

Subjects: Four subjects who were diagnosed with CDSRR from the clinical and electrophysiological findings were ascertained at the National Institute of Sensory Organs, National Tokyo Medical Center, Tokyo, Japan and Niigata University, Niigata, Japan. The natural history of these four patients has been partially reported recently [24]. The procedures used were approved by the ethics committee of each institution, and all procedures were performed in accordance with the principles of the Declaration of Helsinki. Informed consent was obtained from all experimental subjects for all procedures.

Clinical assessment: A complete medical history was obtained, and a comprehensive ophthalmological examination was performed on all patients. The photophobia and night blindness episode was obtained on direct questioning. The clinical assessments included measurements of the best-corrected visual acuity (BCVA), dilated ophthalmoscopy, color fundus photography, AF imaging, OCT, and electrophysiological recordings. AF images were obtained with the HRA 2 confocal scanning laser ophthalmoscope (Heidelberg Engineering, Heidelberg, Germany; excitation light, 488 nm; barrier filter, 500 nm; field of view, 30×30°) [25]. The OCT images were obtained with SD-OCT (Cirrus HD-OCT, versions 4.5 and 5.1; Carl Zeiss Meditec, Dublin, CA) [26].

Electrophysiological assessments: Full-field ERGs were recorded from the four patients with the minimum standard protocol of the International Society for Clinical Electrophysiology of Vision (ISCEV) [27]. The ERG examination included the following: (i) dark adapted dim flash 0.01 $cd{\cdot}s{\cdot}m^{-2}$ (DA 0.01), (ii) dark adapted bright flash 30.0 $cd{\cdot}s{\cdot}m^{-2}$ (DA 30.0), (iii) light adapted 3.0 $cd{\cdot}s{\cdot}m^{-2}$ at 2 Hz (LA 3.0), and (iv) light adapted 3.0 $cd{\cdot}s{\cdot}m^{-2}$ 30 Hz flicker ERG (LA 3.0 30Hz). The extended protocol included the recording of the dark-adapted ERGs elicited by stimulus intensities of 0.001 $cd{\cdot}s{\cdot}m^{-2}$, 0.01 $cd{\cdot}s{\cdot}m^{-2}$, 0.3 $cd{\cdot}s{\cdot}m^{-2}$, 3.0 $cd{\cdot}s{\cdot}m^{-2}$, and 30.0 $cd{\cdot}s{\cdot}m^{-2}$. Two of the four patients were also recorded with the extended protocol. An excessive or disproportionate increase in the dark adapted b-wave with increasing flash intensity was assessed in these two patients, according to the previous report [9].

Mutational screening: After informed consent was obtained, blood samples were collected in EDTA tubes from each subject, and the DNA was extracted with a DNA extraction kit (QIAamp DNA Blood Maxi Kit; Qiagen, Venlo, the Netherlands). All exons and exon–intron boundaries were amplified with polymerase chain reaction (PCR), and the primer sequences used are shown in Table 1. PCR was performed with 20 µl volume containing 0.5 Unit Taq polymerase (PrimeStar GXL DNA polymerase, Takara, Tokyo, Japan). The sequence was determined based on the dideoxy terminator method using an ABI PRISM 3100×l Genetic Analyzer (Applied Biosystems, Foster City, CA) according to the manufacturer's protocol. The SeqScape Software version 2.5 (Applied Biosystems) was used to analyze the sequence alignment. Bidirectional Sanger sequencing was also performed in other family members of the proband, to confirm the segregation of the alleles.

Molecular genetic analyses: All of the missense variants identified were analyzed using two software prediction programs, Sorting Intolerant from Tolerance (SIFT) and PolyPhen2 [28,29]. The predicted effects on splicing of all missense variants were assessed with the Human Splicing finder program version 2.4.1. The allele frequency of each variant was estimated with the Exome Variant Server (NHLBI Exome Sequencing Project, Seattle, WA). A multiple sequence alignment program for DNA or proteins, the Clustal Omega, was applied to confirm an evolutionary conservation. Likely non-disease-causing variants (polymorphisms)

Table 1. Primer Sequences and Conditions for *KCNV2* Mutational Screening.

Primer	Sequence (5'–3')	Product size (bp)	PCR annealing (°C)
E1aF	AGGACCTGAGAAGGGGCAGCT	831	71
E1aR	TCCAGGAGGCGGAGGAACTCT		
E1bF	CCCTGCTGTCCACGCTGAATG	799	71
E1bR	CAGCGTGGGTAAGGTGGGTCA		
E1cF	AAGATCCAGCACGAGCTGCGC	841	65
E1cR	ATGGATGTCAAAAGTGGTGGA		
E2aF	AGCTTCTGTTCTTTTCATGAC	624	63
E2aR	GTCTCATAGTTGCTCTGTGTT		

bp = base pairs.

were also analyzed with the same protocol applied to likely disease-causing variants.

RESULTS

The demographic features of the four individuals from three families with CDSRR are summarized in Table 2. There were two siblings (patients 1 and 2) in one family and one case in each of the two families (patients 3 and 4). The pedigree of each family is shown in Figure 1, and a consanguineous marriage was present in family 3.

Clinical findings: The age of the patient at the time of the examination was 23, 17, 21, and 17 years with the age of disease onset at 9, 5, 3, and 2 years (Table 2). Three patients complained of photophobia (patients 1, 2, and 4), and all four patients had night blindness. Patient 4 had had mild nystagmus since age 2 years. The decimal BCVA of the four patients ranged from 0.08 to 0.8, and the BCVA of patients 1 and 2 was better than 0.7 in each eye.

The findings obtained from the color fundus photographs, AF images, and SD-OCT images are summarized in Figure 1 and Table 2. The fundus photographs showed mottling of the RPE at the macula in all four patients with subtle patchy granular flecks at the macula in patient 3. A ring enhancement of the AF signal was detected in the AF images of all four patients; three subjects had it centered on the fovea (patients 1, 2, and 3), and one had it at the parafovea (patient 4). In patient 3, the ring enhancement at the fovea was surrounded by patchy granular foci of the high AF signal at the macula.

SD-OCT demonstrated abnormalities in the outer retinal layers in all four patients. The cone outer segment tip line was absent in the macular area in all patients. The photoreceptor inner and outer segment junction line was discontinuous at the fovea in patients 3 and 4, and thinning of the outer retina was detected at the fovea in all four patients.

Electrophysiological assessments: The electrophysiological findings are summarized in Table 3, and the ERGs are shown in Figure 2. The full-field ERGs were recorded with the minimum ISCEV standard from patients 2 and 3, and extended protocol full-field ERGs including the dark-adapted ERGs elicited by an intensity series were obtained from patients 1 and 4.

The dark adapted b-wave amplitude elicited by a stimulus intensity 0.01 (DA0.01) was delayed and decreased in patients 3 and 4, but was normal but delayed in patient 1. The responses for DA0.01 were undetectable in patient 2. An excessive increase in the b-wave for the extended protocol was found in two patients, 1 and 4. In addition, the a-wave was square-shaped with a supernormal b-wave elicited by stimulus intensity 30.0 (DA 30.0) in all four patients. The photopic ERGs (LA 3.0 and LA 3.0 30Hz) were decreased in all four patients (Table 3 and Figure 2).

Molecular genetics: The molecular genetic findings are summarized in Table 2 and Appendix 1. Likely disease-causing variants in *KCNV2* were identified in all four patients. The four likely disease-causing variants were p.Arg27His, p.Cys177Arg, p.Arg206Pro, and p.Gly461Arg (Appendix 1), and two likely non-disease-causing variants (polymorphisms) were p.Gly61Gly and p.Ala265Ala (Appendix 2). The segregation of each allele was confirmed by screening of other family members for all these variants.

Detailed molecular results including in silico analysis to assist in predicting the pathogenicity of the four disease-causing variants identified are shown in Appendix 1. All of the four likely disease-causing variants were single nucleotide changes with one amino acid substitution (missense), i.e., p.Arg27His, p.Cys177Arg, p.Arg206Pro, and p.Gly461Arg. Compound heterozygosity for the two alleles, p.Cys177Arg and p.Gly461Arg, in patients 1, 2, and 3 and homozygosity for the complex alleles, p.Arg27His and p.Arg206Pro, in patient

Table 2. Summary of demographics, clinical findings and molecular status for four Japanese patients with *KCNV2*-retinopathy

Pt, FM, gender	Onset of disease, age at examination (years)	VA		Fundus		AF		OCT		Mutation status
		RE	LE	RPE mottling	Subtle patchy granular flecks	Ring enhancement	Patchy granular foci of high signal	Absence of COST	Deficit of IS/OS	
1, 1, F	9, 23	0.7	0.8	Macula	ND	Fovea	ND	Fovea	ND	Compund heterozygous [c.529 T>C, p.Cys177Arg]; [c.1381G>A, p.Gly461Arg]
2, 1, M	5,17	0.7	0.7	Macula	ND	Fovea	ND	Fovea	ND	Compund heterozygous [c.529 T>C, p.Cys177Arg]; [c.1381G>A, p.Gly461Arg]
3, 2, F	3,21	0.1	0.1	Macula	Macula	Fovea	Macuala	Macula	Fovea	Compund heterozygous [c.529 T>C, p.Cys177Arg]; [c.1381G>A, p.Gly461Arg]
4, 3, F	2, 17	0.1	0.08	Macula	ND	Para-fovea	ND	Macula	Fovea	Complex homozygous [c.80 G>A, p.Arg27His]; [c.617 G>C, p.Arg206Pro]

Pt = Patient; FM = family number; VA = logMAR visual acuity; RE = right eye; LE = left eye; RPE = retinal pigment epithelium; AF = autofluorescence; COST = cone outer segment tip line; IS/OS = photoreceptor inner and outer segment junction; ND = not detected. The affected area of each finding is based on the color fundus photographs, AF images, and the OCT images in each column.

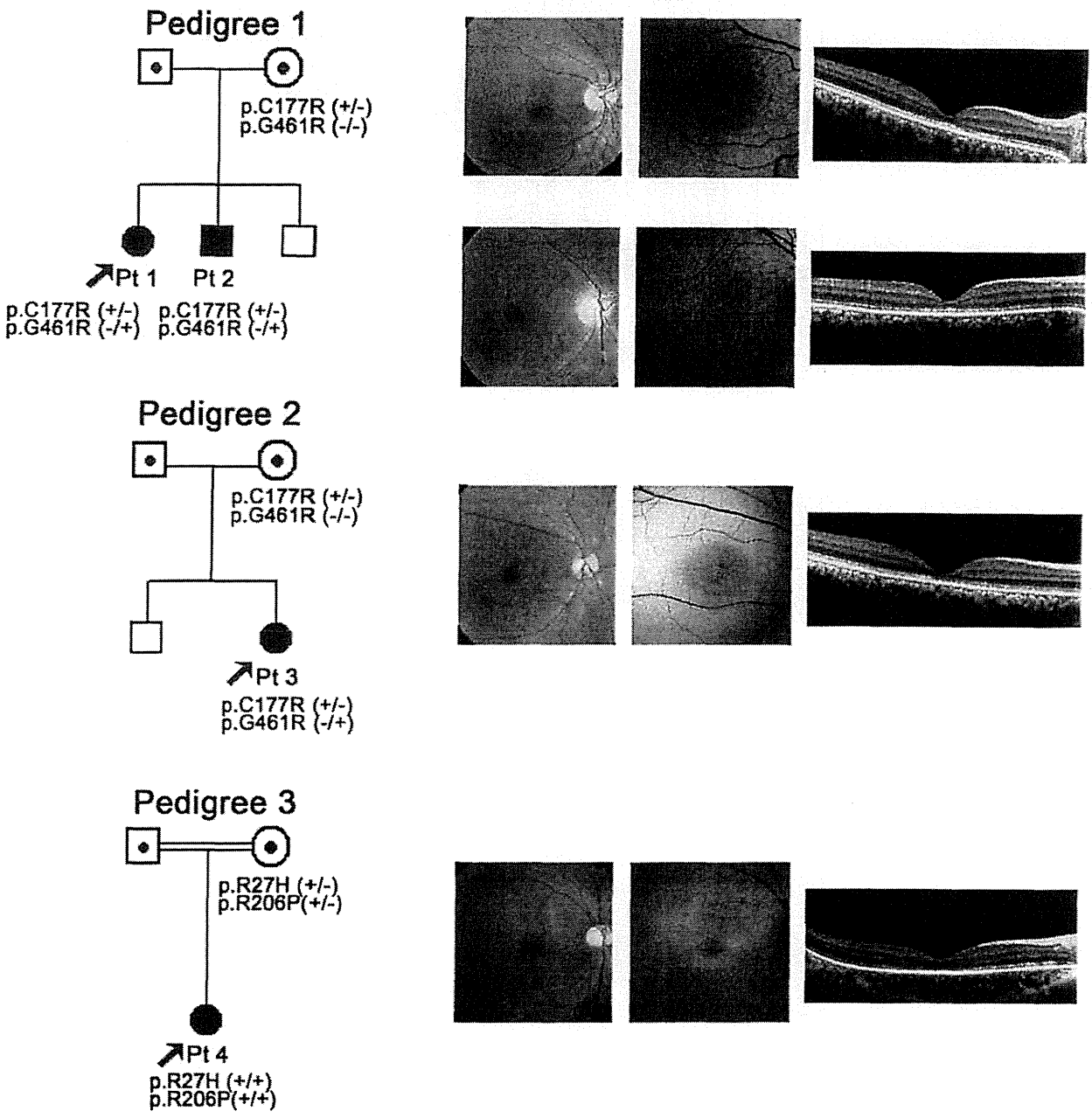

Figure 1. Pedigree and retinal imaging of each patient with potassium channel, subfamily V, member 2 retinopathy. Pedigrees with molecular status of the three families with potassium channel, subfamily V, member 2 (*KCNV2*) retinopathy are shown on the left. Retinal images including color fundus photographs, autofluorescence images, and spectral domain optical coherence tomography are presented on the right. Images of patient 1 (top row), patient 2 (second row from top), patient 3 (third row from top), and patient 4 (bottom row) are shown.

4 were revealed by the segregation analyses. The p.Gly461Arg variant has been reported, and the p.Arg27His, p.Cys177Arg, and p.Arg206Pro variants are putative novel. In silico analysis revealed an "intolerant" protein function or a "probably or possibly damaged" protein but no effect on splicing in the three putative novel variants (SIFT, Poplyphen2, and Human Splicing finder; Appendix 1). The reported missense variant, p.Gly461Arg, with possibly affecting splicing was detected in six out of 13,006 individuals of the Exome Variant Server; the three novel variants, p.Arg27His, p.Cys177Arg, and

Molecular Vision 2013; 19:1580-1590 <http://www.molvis.org/molvis/v19/1580>

Table 3. Electrophysiological Findings of Four Japanese Patients with KCNV2-retionpathy

Pt	DA 0.01		DA 30.0				Square shaped a-wave	Excessive enlargement of b-wave in the extended protocol	LA 3.0			LA 3.0 30Hz		
			A-wave		B-wave				A-wave	B-wave		B-wave		
	Amp (μv)	PT (ms)	Amp	PT	Amp	PT			Amp	PT	Amp	PT	Amp	PT
1	N	Del	N	Del	Super N	NA	(+)	(+)	Sub N	Del	Sub N	UD	UD	UD
2	UD	UD	N	Del	Super N	NA	(+)	NA	Sub N	Del	Sub N	Del	Sub N	Del
3	Sub N	Del	N	Del	Super N	N	(+)	NA	Sub N	Del	Sub N	Del	Sub N	N
4	Sub N	Del	N	Del	Super N	NA	(+)	(+)	Sub N	Del	Sub N	Del	Sub N	Del

Pt = patient; Amp = amplitude; PT = peak time; N = normal; UD = undetectable response; Sub N = subnormal; Del = delayed response; Super N=supernormal response; NA = not available. Full-field electroretinography (ERG) incorporating the standards of the International Society for Clinical Electrophysiology of Vision (ISCEV) included: (i) dark adapted dim flash 0.01 cd•s•m^{-2} (DA0.01), (ii) dark adapted bright flash 30.0 cd•s•m^{-2} (DA30.0), (iii) light adapted 3.0 cd•s•m^{-2} at 2 Hz (LA 3.0), and (iv) light adapted 3.0 cd•s•m^{-2} 30 Hz flicker (LA 3.0 30 Hz). The extended protocol also included the recording of dark adapted responses to an intensity series of flashes in order to detect an excessive enlargement of dark adapted b-wave (patients 1 and 4).

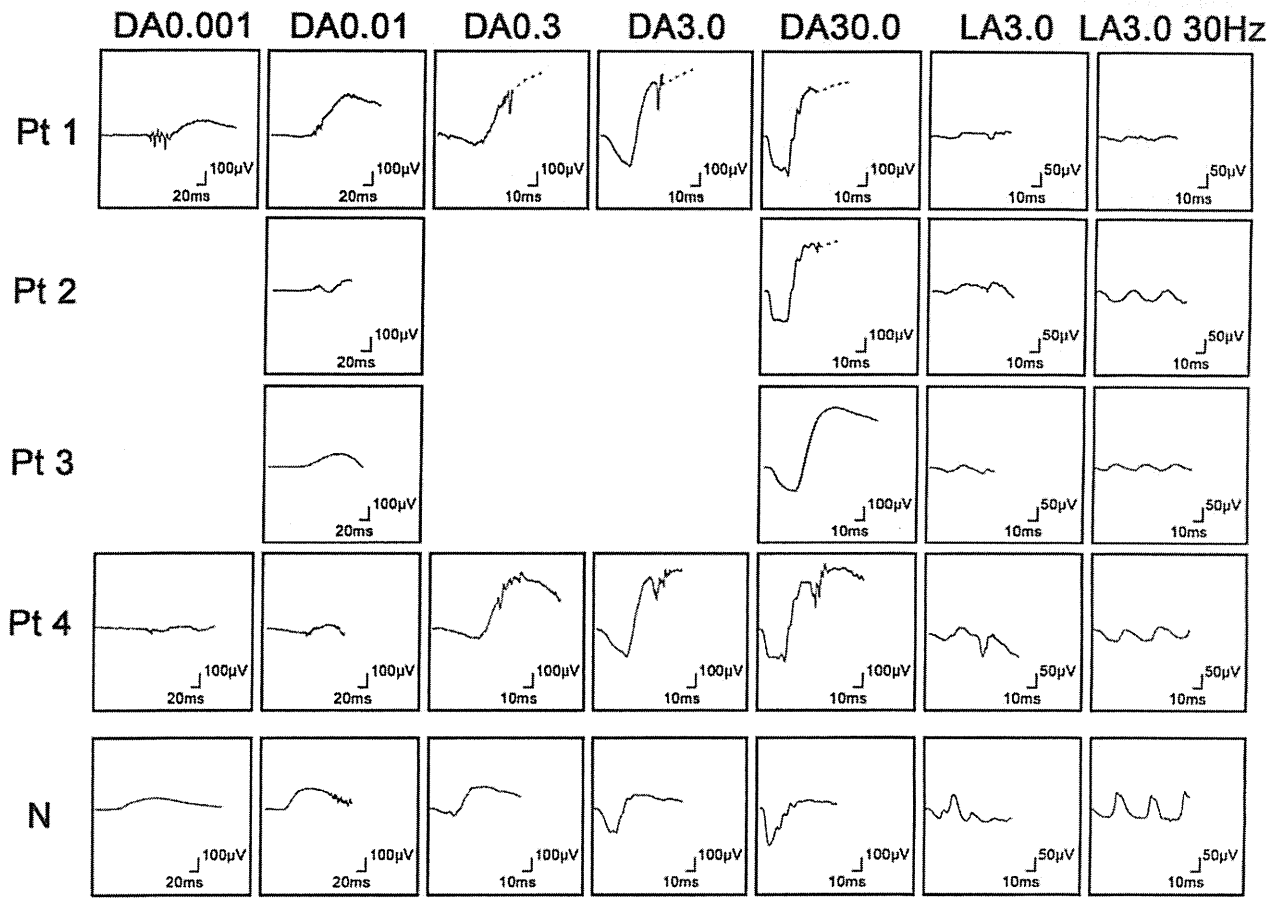

Figure 2. Electrophysiological findings of each patient with potassium channel, subfamily V, member 2 (*KCNV2*) retinopathy. Full-field electroretinograms (ERGs) of patient 1 (top row), patient 2 (second row), patient 3 (third row), and patient 4 (forth row) are shown. The ERGs from a normal control (bottom row) are also shown for comparison. All four patients underwent full-field ERG testing with the minimum standards of the International Society for Clinical Electrophysiology of Vision (ISCEV): (i) dark adapted dim flash 0.01 cd•s•m^{-2} (DA 0.01), (ii) dark adapted bright flash 30.0 cd•s•m^{-2} (DA 30.0), (iii) light adapted 3.0 cd•s•m^{-2} at 2 Hz (LA 3.0), and (iv) light adapted 3.0 cd•s•m^{-2} 30 Hz flicker ERG (LA 3.0 30Hz). The extended protocol was applied to two subjects (patients 1 and 4), including the recording of dark-adapted ERGs to an intensity series of flashes; 0.001 cd•s•m-^{2}, 0.01 cd•s•m^{-2}, 0.3 cd•s•m^{-2}, 3.0 cd•s•m^{-2}, and 30.0 cd•s•m^{-2}.

p.Arg206Pro, were not identified. Three missense variants, p.Arg27His, p.Cys177Arg, and p.Arg206Pro, were highly conserved among the orthologs, and one missense variant, p.Gly461Arg, was completely conserved (Figure 3).

A model of the *KCNV2* protein structure showing the approximate position of the missense disease-causing variants identified is presented in Figure 4. The KCNV2 protein comprises 545 amino acids and contains an N-terminal A and B box (NAB) and six transmembrane domains, (S1–S6), with a K selective motif, GlyTyrGly, in the pore-forming loop (P loop) between S5 and S6 [18]. One variant is located within the N-terminus (p.Arg27His), two variants, p.Cys177Arg and p.Arg206Pro, within the NAB, and one variant, p.Gly461Arg, within the P-loop.

Detailed molecular results of two non-disease-causing variants (polymorphisms) including the in silico analyses are summarized in Appendix 2. These two homozygous variants, p.Gly61Gly and p.Ala265Ala, were synonymous changes in the cording region and were predicted to be benign or have no effect on splicing (Polyphen2 and Human Splicing finder program analysis). Both were present in a high number of chromosomes in the Exome Variant Server database (7647/13006 for p.Gly61Gly and 5636/13006 for p.Ala265Ala, respectively).

Figure 3. Multiple alignment of eight species of potassium channel, subfamily V, member 2 orthologs. The amino acid-sequence alignment is numbered in accordance with the *Homo sapiens* potassium channel, subfamily V, member 2 (*KCNV2*) sequence (ENSP00000371514). The positions of mutated residues, Arg27 (c.80 G>A, p.Arg27His), Arg177 (c.529 T>C, p.Cys177Arg), Arg206 (c.617 G>C, p.Arg206Pro), and Gly461 (c.1381 G>A, p.Gly461Arg), are highlighted. The alignment was performed with the Clustal Omega program, and the asterisk indicates a completely conserved residue.

DISCUSSION

Our results showed the molecular genetic characteristics of four Japanese patients with CDSRR, which, to the best of our knowledge, is the first report of these characteristics of *KCNV2* retinopathy in an East Asian population. Our four patients harbored the likely disease-causing variants in *KCNV2*. Compound heterozygosity for two alleles, p.Cys177Arg and p.Gly461Arg, in three patients and homozygosity for two complex alleles, p.Arg27His and p.Arg206Pro, in one subject were confirmed. Three of the four variants, p.Arg27His, p.Cys177Arg, and p.Arg206Pro, were novel, which indicates all genotypes identified in our series have never been described before.

The clinical and electrophysiological characteristics of our four patients were similar to those of reported patients [8-11,13,14,17,18]. Additionally, all four patients presented with a decrease in central vision whose onset was in the first decade of life with minimal fundus changes and a characteristic ring enhancement of the AF signal (Table 2 and Figure 1). These findings are also in accordance with earlier reports [9-12,14]. SD-OCT demonstrated a discontinuous or absent inner and outer segment junction line in two patients

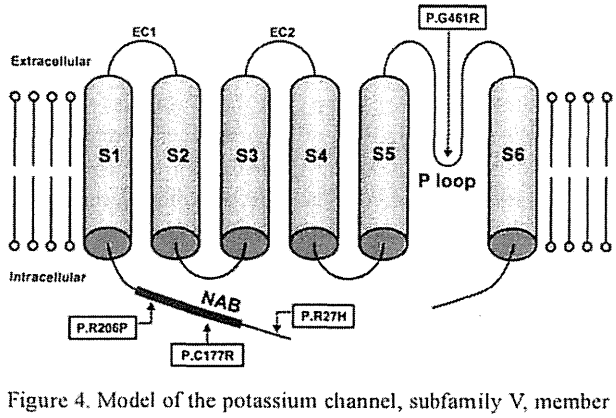

Figure 4. Model of the potassium channel, subfamily V, member 2 protein structure. A schematic representation of the potassium channel, subfamily V, member 2 (*KCNV2*) subunit of the K channel is drawn showing the approximate position of missense disease-causing variants identified in this study. The *KCNV2* protein consists of an N-terminus, an N-terminal A and B box (NAB), and six transmembrane domains (S1–S6), with two extracellular loops (EC 1, 2) and a K selective motif, GlyTyrGly, in the pore-forming loop (P loop) between S5 and S6.

as previously reported [10]. In addition, the absence of the cone outer segment tip line at the macular region was also confirmed in all four patients.

The pathognomonic electrophysiological features were demonstrated in all four patients, viz., delayed and reduced photopic ERGs, delayed ERGs for DA 0.01, and a square-shaped a-wave with a supernormal b-wave for DA 30.0 (Table 3 and Figure 2). An excessive increase in the b-wave for the DA ERGs to an intensity series of flashes was also confirmed in patients 2 and 3. Therefore, the unique rod system abnormalities were identical to those reported for *KCNV2* retinopathy [9,14].

Compound heterozygosity for two alleles, p.Cys177Arg and p.Gly461Arg, was found in patients 1, 2, and 3. The p.Gly461Arg with relatively higher allele frequency affects the third residue of the ultraconserved-GYG-tripeptide motif that acts as an ion selectivity filter in the K channel's pore-forming loop, P loop, between S5 and S6 (Figure 4) [30]. The clinical effect of p.Gly461Arg was well characterized earlier [10,16,17]. Friedburg et al. reported that three siblings with homozygous p.Gly461Arg had a relatively severe phenotype with an early onset and nystagmus at <5 years of age, visual acuity decrease (0.1–0.25, constantly), minimal fundus changes, ring enhancement at the foveal AF image, and an excessive increase in the b-wave for scotopic ERGs to an intensity series [17]. In contrast to the previous reports on homozygous patients, the three patients with heterozygous p.Gly461Arg in our series did not have nystagmus, and two of our patients had less severe BCVA decrease (0.7–0.8). These findings imply that the phenotype of the compound heterozygous for p.Gly461Arg and p Cys177Arg could have a less severe phenotype than those homozygous for p.Gly461Arg. It is of interest that the phenotypic spectrum, compound heterozygous for p.Gly461Arg and p Cys177Arg, was also observed in our series. Two relatively mild phenotypes were observed in the two siblings in our series (patients 1 and 2). In addition, one relatively severe phenotype, with more severe visual acuity decrease (0.1) and photoreceptor/RPE abnormalities at the macula, was detected in patient 3.

Three of the new disease-causing missense variants were located within the N-terminal region of the protein (Figure 4): p.Arg27His within the N-terminus and p.Cys177Arg and p.Arg206Pro within NAB. p.Cys177Arg was completely segregated, and the predicted pathogenesis and evolutionary conservation were confirmed. The coexistence of two likely disease-causing variants, p.Arg27His and p.Arg206Pro, on the same chromosome was also identified in our series with segregation analyses. The patient who was homozygous for these two complex variants had a severe phenotype, with an early onset (2 years), nystagmus, and severe visual acuity decrease (0.1 to 0.08). Both variants were predicted to be pathogenic with evolutionary high conservation (Appendix 1and Figure 3). Whether one of these variants is a neutral polymorphisms in cis with disease-causing one, or whether family 4's alleles are complex with two independently damaging missense variants remains to be determined.

To conclude, this study further delineates the molecular genetic findings of *KCNV2* retinopathy. Three putative novel variants were identified in our four Japanese patients with CDSRR, and our findings suggest there may be a distinct spectrum of *KCNV2* alleles in the Japanese population. However, the clinical findings were similar to that of the reported other population. Electrophysiology was fundamental to the diagnosis with pathognomonic findings due to channelopathy. The pathognomonic characteristics may be a useful method of determining the success of clinical therapeutic trials with gene replacement or pharmacological treatments for channelopathy.

APPENDIX 1. RESULTS OF IN SILICO MOLECULAR GENETIC ANALYSIS OF *KCNV2* MUTATIONS IDENTIFIED.

To access the data, click or select the words "Appendix 1." Pt = patient; Hom = homozygous; Het = heterozygous; SIFT = sorting Intolerant from Tolerance; HSF = human splicing finder program; CV = consensus values; EVS = exome variant server; POD = possibly damaging; PRD = probably damaging; ND = not detected. SIFT (version 4.0.4) results are reported to be tolerant if tolerance index ≥ 0.05 or intolerant if tolerance index < 0.05. Polyphen-2 (vision 2.1) appraises mutations qualitatively as Benign, Possibly Damaging or Probably Damaging based on the model's false positive rate. The cDNA is numbered according to Ensemble transcript ID ENST00000382082, in which +1 is the A of the translation start codon. Human splicing finder version 2.4.1 was applied to predict the effect of each variant on splicing. The results from HSF matrix indicate the values for the wild type and mutant sequences. The larger difference of values between the wild type and the mutant sequences indicates the greater change that the variant can affect on the splice site. EVS denotes variants in the Exome Variant Server, NHLBI Exome Sequencing Project, Seattle, WA.

APPENDIX 2. MOLECULAR ANALYSIS OF *KCNV2* POLYMORPHISMS.

To access the data, click or select the words "Appendix 2." Pt = patient; Hom = homozygous; Het = heterozygous; SIFT = sorting Intolerant from Tolerance; HSF = human splicing

finder program; CV = consensus values; EVS = exome variant server.

ACKNOWLEDGMENTS

We are grateful to the patients who kindly agreed to take part in this study and colleagues who referred individuals to us at National Institute of Sensory Organs. We thank Professor Duco I. Hamasaki (Bascom Palmer Eye Institute, Miami, FL) for proofreading. This research is supported in part by research grants from the Ministry of Health, Labor and Welfare, Japan and Grant-in-Aid for Scientific Research from JSPS.

REFERENCES

1. Gouras P, Eggers HM, MacKay CJ. Cone dystrophy, nyctalopia, and supernormal rod responses. A new retinal degeneration. Arch Ophthalmol 1983; 101:718-24. [PMID: 6601944].
2. Alexander KR, Fishman GA. Supernormal scotopic ERG in cone dystrophy. Br J Ophthalmol 1984; 68:69-78. [PMID: 6607068].
3. Yagasaki K, Miyake Y, Litao RE, Ichikawa K. Two cases of retinal degeneration with an unusual form of electroretinogram. Doc Ophthalmol 1986; 63:73-82. [PMID: 3015524].
4. Foerster MH, Kellner U, Wessing A. Cone dystrophy and supernormal dark-adapted b-waves in the electroretinogram. Graefes Arch Clin Exp Ophthalmol 1990; 228:116-9. [PMID: 2186970].
5. Kato M, Kobayashi R, Watanabe I. Cone dysfunction and supernormal scotopic electroretinogram with a high-intensity stimulus. A report of three cases. Doc Ophthalmol 1993; 84:71-81. [PMID: 8223112].
6. Rosenberg T, Simonsen SE. Retinal cone dysfunction of supernormal rod ERG type. Five new cases. Acta Ophthalmol (Copenh) 1993; 71:246-55. [PMID: 8333273].
7. Hood DC, Cideciyan AV, Halevy DA, Jacobson SG. Sites of disease action in a retinal dystrophy with supernormal and delayed rod electroretinogram b-waves. Vision Res 1996; 36:889-901. [PMID: 8736222].
8. Michaelides M, Holder GE, Webster AR, Hunt DM, Bird AC, Fitzke FW, Mollon JD, Moore AT. A detailed phenotypic study of "cone dystrophy with supernormal rod ERG". Br J Ophthalmol 2005; 89:332-9. [PMID: 15722315].
9. Robson AG, Webster AR, Michaelides M, Downes SM, Cowing JA, Hunt DM, Moore AT, Holder GE. "Cone Dystrophy with Supernormal Rod Electroretinogram": A Comprehensive Genotype/Phenotype Study Including Fundus Autofluorescence and Extensive Electrophysiology. Retina 2010; 30:51-62. [PMID: 19952985].
10. Sergouniotis PI, Holder GE, Robson AG, Michaelides M, Webster AR, Moore AT. High-resolution optical coherence tomography imaging in KCNV2 retinopathy. Br J Ophthalmol 2012; 96:213-7. [PMID: 21558291].
11. Vincent A, Robson AG, Holder GE. PATHOGNOMONIC (DIAGNOSTIC) ERGs A Review and Update. Retina 2013; 33:5-12. [PMID: 23263253].
12. Khan AO, Alrashed M, Alkuraya FS. 'Cone dystrophy with supranormal rod response' in children. Br J Ophthalmol 2012; 96:422-6. [PMID: 21900228].
13. Zobor D, Kohl S, Wissinger B, Zrenner E, Jagle H. Rod and Cone Function in Patients with KCNV2 Retinopathy. PLoS ONE 2012; 7:e46762-[PMID: 23077521].
14. Vincent A, Wright T, Garcia-Sanchez Y, Kisilak M, Campbell M, Westall C, Heon E. Phenotypic Characteristics including in vivo Cone Photoreceptor Mosaic in KCNV2-Related 'Cone Dystrophy with Supernormal Rod Electroretinogram'. Invest Ophthalmol Vis Sci 2013; 30:898-908. .
15. Tanimoto N, Usui T, Ichibe M, Takagi M, Hasegawa S, Abe H. PIII and derived PII analysis in a patient with retinal dysfunction with supernormal scotopic ERG. Doc Ophthalmol 2005; 110:219-26. [PMID: 16328930].
16. Wissinger B, Dangel S, Jagle H, Hansen L, Baumann B, Rudolph G, Wolf C, Bonin M, Koeppen K, Ladewig T, Kohl S, Zrenner E, Rosenberg T. Cone dystrophy with supernormal rod response is strictly associated with mutations in KCNV2. Invest Ophthalmol Vis Sci 2008; 49:751-7. [PMID: 18235024].
17. Friedburg C, Wissinger B, Schambeck M, Bonin M, Kohl S, Lorenz B. Long-term follow-up of the human phenotype in three siblings with cone dystrophy associated with a homozygous p.G461R mutation of KCNV2. Invest Ophthalmol Vis Sci 2011; 52:8621-9. [PMID: 21911584].
18. Wu H, Cowing JA, Michaelides M, Wilkie SE, Jeffery G, Jenkins SA, Mester V, Bird AC, Robson AG, Holder GE, Moore AT, Hunt DM, Webster AR. Mutations in the gene KCNV2 encoding a voltage-gated potassium channel subunit cause "cone dystrophy with supernormal rod electroretinogram" in humans. Am J Hum Genet 2006; 79:574-9. [PMID: 16909397].
19. Czirják G, Toth ZE, Enyedi P. Characterization of the heteromeric potassium channel formed by kv2.1 and the retinal subunit kv8.2 in Xenopus oocytes. J Neurophysiol 2007; 98:1213-22. [PMID: 17652418].
20. Hölter P, Kunst S, Wolloscheck T, Kelleher DK, Sticht C, Wolfrum U, Spessert R. The retinal clock drives the expression of Kcnv2, a channel essential for visual function and cone survival. Invest Ophthalmol Vis Sci 2012; 53:6947-54. [PMID: 22969075].
21. Beech DJ, Barnes S. Characterization of a voltage-gated K+ channel that accelerates the rod response to dim light. Neuron 1989; 3:573-81. [PMID: 2642011].
22. Thiagalingam S, McGee TL, Weleber RG, Sandberg MA, Trzupek KM, Berson EL, Dryja TP. Novel mutations in the KCNV2 gene in patients with cone dystrophy and a supernormal rod electroretinogram. Ophthalmic Genet 2007; 28:135-42. [PMID: 17896311].

23. Wissinger B, Schaich S, Baumann B, Bonin M, Jagle H, Friedburg C, Varsanyi B, Hoyng CB, Dollfus H, Heckenlively JR, Rosenberg T, Rudolph G, Kellner U, Salati R, Plomp A, De Baere E, Andrassi-Darida M, Sauer A, Wolf C, Zobor D, Bernd A, Leroy BP, Enyedi P, Cremers FP, Lorenz B, Zrenner E, Kohl S. Large deletions of the KCNV2 gene are common in patients with cone dystrophy with supernormal rod response. Hum Mutat 2011; 32:1398-406. [PMID: 21882291].

24. Nakamura N, Tsunoda K, Fujinami K, Shinoda K, Tomita K, Hatase T, Usui T, Akahori M, Iwata T, Miyake Y. Long-term Observation over Ten Years of Four Cases of Cone Dystrophy with Super-normal Rod Electroretinogram . Nippon Ganka Gakkai Zasshi 2013; In press.

25. Fujinami K, Tsunoda K, Hanazono G, Shinoda K, Ohde H, Miyake Y. Fundus autofluorescence in autosomal dominant occult macular dystrophy. Arch Ophthalmol 2011; 129:597-602. [PMID: 21555613].

26. Tsunoda K, Usui T, Hatase T, Yamai S, Fujinami K, Hanazono G, Shinoda K, Ohde H, Akahori M, Iwata T, Miyake Y. Clinical characteristics of occult macular dystrophy in family with mutation of Rp111 gene. Retina 2012; 32:1135-47. [PMID: 22466457].

27. Marmor MF, Fulton AB, Holder GE, Miyake Y, Brigell M, Bach M. ISCEV Standard for full-field clinical electroretinography (2008 update). Doc Ophthalmol 2009; 118:69-77. [PMID: 19030905].

28. Ng PC, Henikoff S. SIFT: Predicting amino acid changes that affect protein function. Nucleic Acids Res 2003; 31:3812-4. [PMID: 12824425].

29. Adzhubei IA, Schmidt S, Peshkin L, Ramensky VE, Gerasimova A, Bork P, Kondrashov AS, Sunyaev SR. A method and server for predicting damaging missense mutations. Nat Methods 2010; 7:248-9. [PMID: 20354512].

30. Heginbotham L, Lu Z, Abramson T, MacKinnon R. Mutations in the K+ channel signature sequence. Biophys J 1994; 66:1061-7. [PMID: 8038378].

Articles are provided courtesy of Emory University and the Zhongshan Ophthalmic Center, Sun Yat-sen University, P.R. China. The print version of this article was created on 20 July 2013. This reflects all typographical corrections and errata to the article through that date. Details of any changes may be found in the online version of the article.

Original Paper

Ophthalmic Research

Ophthalmic Res
DOI: 10.1159/000356688

Received: July 29, 2013
Accepted: September 25, 2013
Published online: ■■■

Comparisons of Pattern Visually Evoked Potentials Elicited by Different Response Time Liquid Crystal Display Screens

Celso Soiti Matsumoto[a, b] Kei Shinoda[a] Harue Matsumoto[b] Hideaki Funada[c] Kakeru Sasaki[a] Haruka Minoda[a] Atsushi Mizota[a]

[a]Department of Ophthalmology, Teikyo University School of Medicine, Tokyo, [b]Matsumoto Eye Clinic, Tokushima, and [c]Engineering Department, Tomey Corporation, Nagoya, Japan

Key Words
Liquid crystal display monitor · Visually evoked potentials · Cathode ray tube · Flash visually evoked potentials · Pattern reversal visually evoked potentials · Contrast · Response time

Abstract
Purpose: To evaluate the usefulness of a liquid crystal display (LCD) with higher driving frequency and shorter response time (2 ms) as a visual stimulator to elicit pattern reversal visually evoked potentials (p-VEPs). ***Method:*** p-VEPs were recorded from 12 eyes of 12 healthy volunteers (28.3 ± 9 years). The p-VEPs elicited by a conventional cathode ray tube (CRT) screen were compared to those elicited by a high-speed LCD screen (2-ms LCD, GD245HQbid, Acer, Taipei, Taiwan). The luminance changes of each monitor were measured with a photodiode. ***Results:*** During the reversal phase the luminance of the 2-ms LCD screen with 97% contrast was transiently reduced, which can elicit an electroretinogram (ERG) and therefore a flash VEP. The 2-ms LCD with 81% contrast checkerboard had a minimal luminance reduction during the reversal phase, and therefore no ERGs were elicited. No significant differences in the amplitude of P100 and the implicit times of N75 and P100 were observed in the p-VEPs elicited by a CRT or the 2-ms LCD screens as stimulators. ***Conclusion:*** The luminance change can elicit flash VEPs, and this artifact can be minimized by using a 2-ms LCD screen with reduced contrast of the checkerboard stimulus.

Introduction

Cathode ray tube (CRT) monitors have been replaced by liquid crystal display (LCD) screens as visual stimulators to elicit pattern reversal visually evoked potentials (p-VEPs). However, LCDs have an inherent problem as visual stimulators because they take several milliseconds for the crystal molecules to change their alignment to permit the light to pass through the polarizing filter of the LCD (http://www.sharp.co.jp/products/lcd/tech/s2_1.html) [1, 2].

The results of earlier investigators [3–5] and our studies [6] showed that the p-VEPs elicited by LCD screens had longer implicit times than those elicited by CRT screens. This was partly due to a transient reduction of the mean luminance of the entire LCD screen at the time of the reversal. This reduction in the luminance was significant because it could elicit electroretinograms (ERGs) and flash VEPs. We named this phenomenon the flash effect. Our earlier study [6] showed that the luminance changes of the LCD were not symmetrical when going

KARGER

E-Mail karger@karger.com
www.karger.com/ore

0030–3747/13/0000–0000$38.00/0

Kei Shinoda, MD, PhD
Department of Ophthalmology
Teikyo University School of Medicine
Kaga 2-11-1, Itabashi-ku, Tokyo 173-8605 (Japan)
E-Mail shinodak@med.teikyo-u.ac.jp

from black to white or from white to black. We suggested that one solution to the flash effect might be to optimize the contrast of the checkerboard luminance of the LCD screens [6]. However, it would be necessary to reduce the contrast to 65% for some of the commercial monitors to completely eliminate the flash effect. Unfortunately, this exceeds the limit of the International Society for Clinical Electrophysiology of Vision (ISCEV) standard which recommends that the contrast be not less than 80%.

Because the time delay in the luminance change depends on the driving frequency of the LCD, we assumed that a high-speed LCD with a 2-ms response time would have less reduction in the luminance and thereby achieve better performance as a stimulator to elicit p-VEPs.

Thus, the purpose of this study was to compare the luminance profile of LCDs with a 2-ms response time to the more widely used LCD displays with a 5-ms response time. We also compared the p-VEPs elicited by these two types of monitors.

Subjects and Methods

Subjects

Twelve eyes of 12 healthy volunteers, who did not have any ocular diseases except for refractive errors, were studied. There were 4 men and 8 women whose mean age was 28.3 ± 9 years (±standard deviation) with a range of 22–46 years. The guidelines of the Declaration of Helsinki were followed, and this study was approved by the Institutional Review Board of Teikyo University. An informed consent was obtained from all of the subjects after an explanation of the purpose of the study, procedures to be used and possible complications.

Methods

Measurement on Luminance of Single Check

To determine the time delay of each monitor, the luminance change of a single check was measured with a photodiode (S1133, Hamamatsu Photonics Co. Ltd., Hamamatsu, Japan). The photodiode was attached in the upper left corner of the single check.

In addition, the luminances at the 4 corners and 1 point at the center of the entire checkerboard screen were measured with a luminance meter (CA-100S, Konica Minolta Inc., Osaka, Japan). We confirmed that the variation from the center to the periphery was within 20% for each of the monitors, which complies with the standards of the ISCEV guidelines [7].

The luminance and contrast of both the CRT and LCD screens were matched. The contrast between the black and white checks was calculated with the Michaelson contrast formula [8].

Pattern Reversal Stimuli

The visual stimulus was a black-and-white checkerboard generated either on a CRT screen (17 inches, 320 × 230 mm, S710, Compaq Computer Co., USA), an LCD screen (17 inches, 340 × 270 mm, E170Sc, Dell, Tex., USA) or another LCD screen (23.6 inches, 521 × 293 mm, GD245HQbid, Acer, Taipei, Taiwan). Because the aspect ratio of the 2-ms response LCD screen did not match the checkerboard stimulus pattern, the checkerboard pattern of 370 × 275 mm in size was displayed at the center of the 2-ms LCD display by an analog-digital converter (CP-293 Cypress Technology Enterprises Inc., Calif., USA). The overall size of the CRT screen was 19 × 28°, that for the 5-ms response LCD was 21 × 26.2° and that for the 2-ms response LCD screen was 22 × 29°. Both LCD screens are commercially available. The response time was 5 ms for one LCD screen (5-ms response LCD) and 2 ms for the other (2-ms response LCD) according to the specifications of the manufacturers. The response time was defined as the time it takes 1 pixel to turn from white to black or from black to white. Others consider the response time as the time required to change from gray to gray [1, 2].

The maximum contrast was 97% for the experiments. The check size was 0.25° at an observation distance of 70 cm, and the reversal rate was 3.0 reversals/s. The resolution of each monitor was 800 × 600 pixels, and the vertical frequency was 59.8 Hz.

We found that the time delay for the luminance change in the 5-ms response LCD screen led to a transient reduction in the average luminance which we named the flash effect. In our earlier study, we showed that the flash effect was important because it could elicit ERGs and flash VEPs when the stimuli were presented through a diffuser (Kuraray, DFA2-P, Tokyo, Japan) [6]. We compared the flash effect for the 5-ms and 2-ms response LCD screens. Because we found a weak flash effect even with the 2-ms response LCD screen, the contrast of the checkerboard pattern was reduced from 97 to 80% to minimize the flash effect.

p-VEP Recordings

All recordings were performed under dim room lights with an illumination of about 104 lx. The subjects were preadapted to the room lighting before beginning the recordings. A small black fixation point was positioned at the corners of the 4 central checks of the stimulus screen, and the subjects were instructed to fixate the point or the center of the screen and to try not to blink. The subjects wore their best refractive correction, and all recordings were monocular.

The recording electrode was placed on the inion (Oz), and the reference electrode was placed at Fz. The ground electrode was placed on the right earlobe. Signals were amplified 4,000 times (LE-4000, Tomey Corporation, Nagoya, Japan) and bandpass filtered from 1.0 to 100 Hz. The sampling rate was 1.0 kHz, and 128 responses were averaged. The recordings were performed at least twice to determine the repeatability. In addition, the measurements for each subject were performed twice with a 1-week interval to determine the intermeasurement variability.

Data Analyses

The P2 amplitude was measured between N75 and P100, and the implicit times of N75 (N1 implicit time) and P100 (P2 implicit time) were also measured. Student's t tests were used to determine the significance of differences of each parameter. A $p < 0.05$ was taken to be significant.

Results

Luminance Changes of Checkerboard for Each Monitor

The changes in the luminance are plotted against time in figure 1. The input lag, the time between the signal input

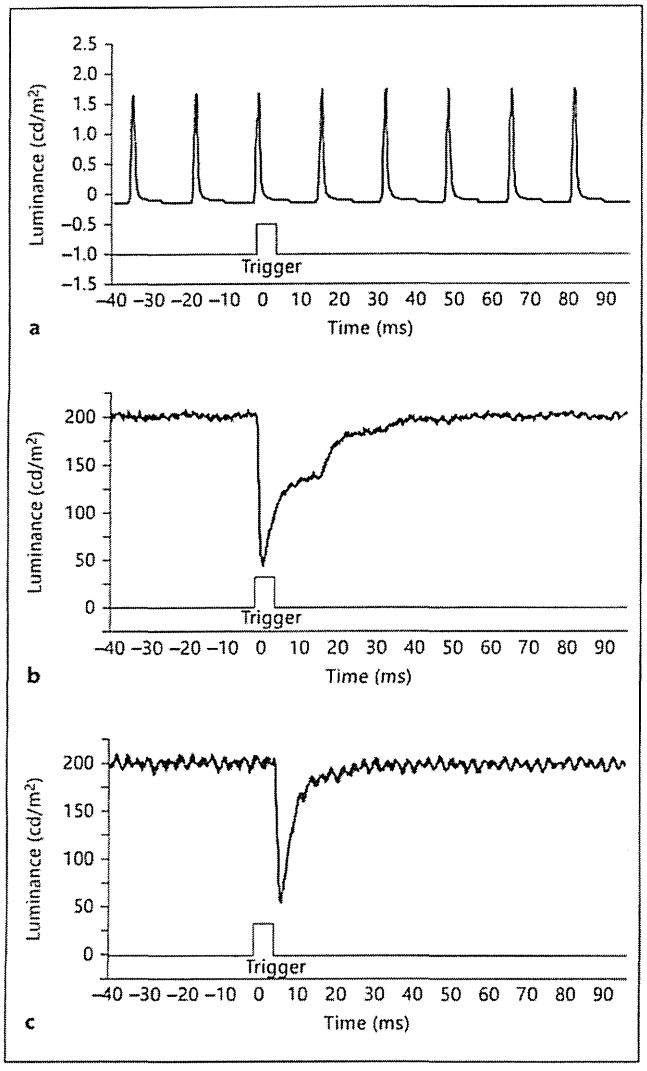

Fig. 1. Changes in the average luminance of a single check of each monitor during a pattern reversal. There is no real luminance change in a single check because half of the checks are changing in the opposite direction. The figure represents luminance changes of the entire screen. **a** Luminance changes of the CRT screen. There is no change in the total luminance (y-axis) during time (x-axis). **b** Luminance changes of a conventional 60-Hz LCD display which we refer to as 5-ms response LCD. There is an abrupt change of the luminance (y-axis) at the time of reversal of the checkerboard (x-axis). The descending point of the luminance reduction begins with a 1.2-ms delay after the trigger signal which is called the input lag. **c** Luminance changes of a conventional 120-Hz LCD screen which we call the 2-ms response LCD screen. An abrupt change of the luminance can be seen. The reduced luminance recovered to the baseline faster than that with the 5-ms response LCD. This may result in a weaker flash effect compared to the 5-ms response LCD. The input lag was 13.7 ms.

to the display to the time a change in luminance is detected, was the longest for the 2-ms response LCD. A burst of pulses at 60 Hz was delivered to the CRT monitor to change the luminance of the white checks, and a square wave pulse was delivered to the LCD screens. No significant delay was detected during the check reversal in the CRT monitor.

During the reversal phase, the luminance change was delayed in the 5-ms response LCD screen especially from black to white. The delay was caused by the time for the crystal liquid molecules to line up to permit light transmission through the polarizing layers. The change in the luminance on the ascending slope was unique to a specific LCD screen. The delay was asymmetrical between black to white and white to black which led to a transient reduction in the mean luminance of the entire screen. However, because the recovery period was rapid in the 2-ms response LCD, the transient reduction was minimal compared with that of the 5-ms response LCD screen.

Nagy et al. [5] reported that the p-VEPs elicited by LCD displays had longer implicit times. The delay was attributed to the total temporal differences between the LCD's electronic input and radiometric output signals, caused by the response time and the input lag. When referred to the trigger, the input lag was measured to be approximately 1.2 ms for the 5-ms response LCD and 13.7 ms for the 2-ms response LCD screens used in this study. The input lag is the time between the input signal leaving the video card and the image appearing on the screen [5, 9]. The reason for this is that the input signal is usually further processed at the display level before it appears on the screen. The image-processing technologies and processing times can vary with the manufacturer, display type and setup parameters, such as the resolution, color settings and internal processes [10]. Because the input lag was constant for the monitors used, it was subtracted from the implicit time in the analyses of the p-VEPs (see 'Comparison of p-VEP components' below).

Pattern Reversal Stimuli to Minimize the Flash Effect

The changes in the luminance of the checks on the LCD screen with contrasts of 97 and 81% are shown in figure 2. The transient changes in the luminance were significantly smaller with 81% contrast.

When a contact lens electrode was placed on the cornea and the stimulus pattern on the monitor was screened by a diffuser, ERGs could be recorded but when the diffuser was placed in front of the CRT monitor, no ERGs were elicited. When the diffuser was placed before the LCD screen with 97% contrast, an ERG was elicited with a positive peak at about 100–120 ms (fig. 3). When the